Impact of chitosan on CS/TiO$_2$ composite system for enhancing its photocatalytic performance towards dye degradation

Saba Afzal[a,b,*], Rabia Naeem[c], Bibi Sherino[b], Nusrat Nabi[b], Farida Behlil[b], Nurhidayatullaili Muhd Julkapli[a]

[a]*Nanotechnology and Catalysis Research Center (NANOCAT), University of Malaya, Kuala Lumpur, Malaysia,*
emails: sag_dec@hotmail.com (S. Afzal), nurhidayatullaili@um.edu.my (N.M. Julkapli)
[b]*Department of Chemistry, Sardar Bahadur Khan Women's University, Quetta, Pakistan, emails: sherinobibi@yahoo.com*
(B. Sherino), nusratmunawarsbku@gmail.com (N. Nabi), farida_behlil@yahoo.com (F. Behlil)
[c]*Department of Chemistry, Government College, University of Lahore, Pakistan, email: rabianaeem49@yahoo.com*

ABSTRACT

Chitosan, supported by titanium dioxide nanocomposite (CS/TiO$_2$) is synthesized using the *in-situ* sol–gel method. The synthesis was carried out at room temperature to obtain CS/TiO$_2$ containing TiO$_2$ in the anatase phase. The prepared samples were characterized by using scanning electron microscopy, X-ray diffraction (XRD), Raman, photoluminescence (PL), and infrared techniques. The modification aims to assess the impact of CS concentration on the structural and photodegradation properties of the resultant composite. The synthesized composite samples are used to evaluate the adsorption photodegradation of Methyl orange as a model pollutant. The composite sample with lower CS concentration (CT1) shows the highest adsorption-photodegradation efficiency which gradually declined by increasing CS content. The high efficiency of CT1 is attributed to its high crystallinity, lower crystallite size, and better e$^-$ – h$^+$ separation as detailed in XRD and PL results. It is undeniable that CS improves the adsorption properties of TiO$_2$ however its optimum concentration is achieved in CT1.

Keywords: Chitosan; TiO$_2$; Adsorption; Photocatalysis; e$^-$ – h$^+$; Methyl orange

1. Introduction

Among nanostructured materials, TiO$_2$ has been proven to be an excellent catalyst in the photocatalytic degradation of a broad range of both organic and inorganic pollutants. As it is an effective catalyst, photostable, non-toxic, frequently abundant, and recyclable catalyst, therefore, receiving much attention, particularly for the treatment of wastewater where it can completely mineralize toxic and non-biodegradable compounds into CO$_2$ and inorganic acid [1,2]. Unlike TiO$_2$, other semiconductors like GaP, CdS, and ZnO cannot be used for environmental purification as they produce toxic by-products during photocatalysis due to their solubility in the solution [3,4]. Similarly, PbS, GaAs, and CdS are toxic and undergo photo corrosion and thus, cannot be used as a catalyst in aqueous media [5,6].

However, there are certain drawbacks associated with nano TiO$_2$ in terms of recycling, low adsorption towards organic pollutants, and agglomeration which declines its photocatalytic activity [3,4]. One way to improve the efficiency of TiO$_2$ is modifying its surface with support materials like SiO$_2$, ZrO$_2$, zeolites, and activated carbons but these series of materials are usually rigid, expensive, and not environmental friendly [5]. The adsorption process mediated by chitosan is the most effective among all

* Corresponding author.

[3]. In general, chitosan is a cationic biopolymer prepared by the N-deacetylation of chitin. It contains plentiful amino (R-NH$_2$) and hydroxyl (OH) groups in the macromolecular chains that facilitate the adsorption of contaminants [7,8]. These R-NH$_2$ and OH groups are also responsible for the binding of chitosan with TiO$_2$ [10]. Chitosan can efficiently prevent TiO$_2$ nanoparticles from agglomeration during growth and is expected to solve the recovery problem of nanocomposite after wastewater treatment [11].

In the current study, the *in-situ* sol–gel method is used for the synthesis of CS/TiO$_2$ nanocomposite. This method not only provides the growth of nanocomposite with the control size distribution of nanoparticles in CS matrix at relatively low temperatures but also controls the interactions between organic and inorganic moieties of a composite at several nanometers, micrometers, and molecular scales. However, an optimal concentration of chitosan is required for the modification of TiO$_2$ to get desired structural properties with enhanced photodegradation results.

Therefore, the present research aims to modify and optimize TiO$_2$ using different CS concentrations for effective photocatalytic degradation studies. *In-situ* sol–gel method is used to synthesize chitosan modified TiO$_2$ as it is expected to enhance its physicochemical properties by producing homogenous dispersion of particles with strong interactions between TiO$_2$ and chitosan matrix. The effect of different chitosan concentrations on TiO$_2$ was assessed towards the photocatalytic degradation of Methyl orange as a model pollutant.

2. Materials and methodology

2.1. Chemicals

CS with medium molecular weight and titanium tetra isopropoxide (TTIP, 97%) purchased from Sigma-Aldrich. Ethanol (99.5%), acetic acid (100%), hydrochloric acid (37%), and Methyl orange were purchased from Merck. All these reagents are of analytical grade and used without further purification. For the preparation of solutions deionized water is used.

2.2. Synthesis of CS-TiO$_2$ nanocomposite

CS modified TiO$_2$ nanocomposites were synthesized by *in-situ* sol–gel method at three varying concentrations of CS (0.1, 0.2, and 0.3 g) and expressed as (CT1, CT2, and CT3, respectively). Solutions of CS solution were prepared by dissolving it in 2% acetic acid under vigorous stirring. TiO$_2$ sol was prepared by dissolving TTIP in ethanol followed by the addition of hydrochloric acid (as an acid catalyst) and water. Then as prepared CS solution is added dropwise into TiO$_2$ sol under vigorous stirring. This solution is kept for aging to get a semisolid which is then washed with deionized water and ethanol several times and dried at 60°C for 12 h.

2.3. Characterization of CS-TiO$_2$ nanocomposite

Morphology of nanocomposite is determined by HRSEM (Quanta 450 FEG). The crystalline size and phase formation of synthesized nanocomposit was assessed by X-ray diffraction with Bruker-Axs, Cu Kα radiation (2θ, 10°–80°). Renishaw-inVia, NIR vibrations from 800 to 50 cm^{-1} is used for Raman and photoluminescence (PL) measurement. Fourier-transform infrared spectroscopy (FTIR) measurements were carried out to confirm the occurrence of functional groups and bonding between TiO$_2$ and chitosan matrix in the range of 400–4,000 cm^{-1}. Furthermore, the absorption data of all the Methyl orange (MO) samples is recorded on UV-VIS, Shimadzu-UV-3101PC in the range of 200–800 nm.

2.4. Photodegradation reaction

The photocatalytic reaction was conducted at room temperature in a quartz cylindrical glass (150 mL). The UV lamp of 365 nm is located at the center of the quartz glass to provide UV irradiation. 100 mL of 10 mg/L of Methyl orange was prepared and used to assess the photoactivity of the composite sample. The process of adsorption was performed under dark conditions for about 30 min in the presence of CS-TiO$_2$ composite samples before the photodegradation process. The absorbance of solution after photodegradation was measured directly by UV-VIS spectrophotometer (UV-3101PC Shimadzu) at a wavelength of 464 nm which is the maximum absorption wavelength of Methyl orange.

3. Results and discussion

3.1. Scanning electron microscopy analysis

Scanning electron microscopy (SEM) images of CS-TiO$_2$ nanocomposites prepared under different chitosan concentrations are presented in Fig. 1. It can be clearly seen that
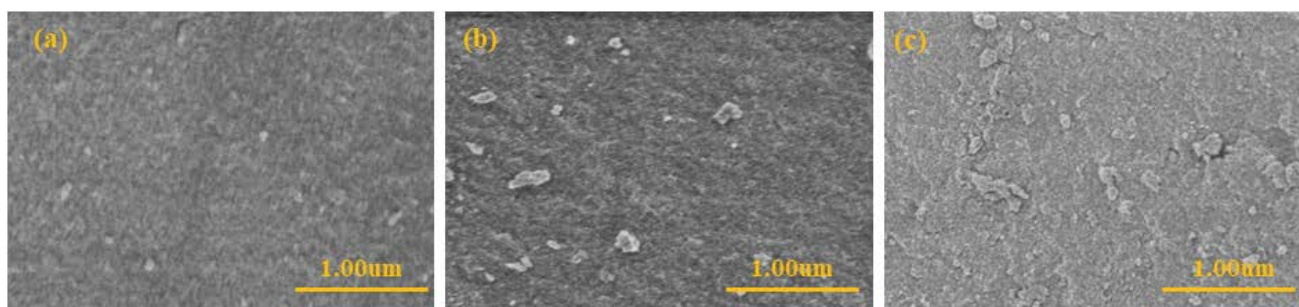
Fig. 1. SEM images of (a) CT1, (b) CT2, and (c) CT3.

most of TiO_2 nanoparticles are covered and merged into the CS matrix which is expected to improve the adsorption mechanism of the catalyst. The surface of catalyst is noticeably rough due to CS layer which is gradually increased due to increase concentration of CS [10,11]. The higher concentration of CS also leads to aggregation as observed in Fig. 1c that resulted in reducing the uniformity of chitosan layer onto TiO_2. The aforementioned morphology is expected to reduce the photocatalytic activity of the catalyst.

3.2. X-ray diffraction analysis

The X-ray diffraction (XRD) spectra of $CS-TiO_2$ (CT1, CT2, and CT3) are shown in Fig. 2. The prominent diffraction peaks in the range of 25°, 38°, and 48° correspond to 101, 112, 200, and 105 planes, respectively. As samples were prepared at room temperature and were not calcined to prevent chitosan degradation at high temperature, therefore, the crystallinity is comparatively low. In Fig. 2 the peak intensities were low however, all these peaks agree well with the tetragonal anatase phase of TiO_2 (JCPDS 01-075-1537) [11]. The inclusion of CS did not bring any peak shift however peak intensity decreased by increasing CS concentration as CS is a polymer and semi crystalline [10,11]. The crystallinity of the composite samples was reduced by increasing CS concentration. Since all three samples were of the anatase phase so it was expected that the sample with high crystallinity performed better in photodegradation studies. The activity of a composite in photocatalytic reactions depends on its phase and crystallinity [13]. The crystallite size (in 101 planes) was calculated by applying the Scherrer's equation [$D = (K\lambda)/\beta\cos)$] and presented in Table 1. The gradual increase in crystallite size is observed by increasing the concentration of CS. As TiO_2 contributes mainly due to crystallinity and its concentration remaining the same in all composite samples. Hence, the samples prepared at higher polymer (CS) concentration caused to reduce the crystallinity with the large crystallite size of the composite. The aforementioned phenomenon will affect the photocatalytic efficiency of the composite sample as the

crystallite size and crystallinity of the catalyst have a great impact on its performance [14]. The composite sample with high crystallinity and small crystallite size (CT1) is expected to perform well in photocatalytic reactions.

3.3. Raman analysis

Raman spectra of CT composite samples (CT1, CT2, and CT3) are shown in Fig. 3. Spectra indicate the prominent peaks around 151, 400, 515, and 639 cm^{-1} correspond to E_g, B_{1g}, A_{1g}, and E_g Raman active modes of anatase TiO_2, well indexed with XRD results [15]. A small band around 2,932 cm^{-1} is due to the presence of the CH_3 group, confirming the presence of CS [16]. The variation in the intensities of Raman bands is in agreement with XRD results. The band intensities gradually decrease with increasing concentration of CS. This variation can be related to respective crystallite sizes and crystallinities of the composite sample. As the Raman signals increase with a decrease in particle size [17].

3.4. Infrared analysis

Infrared spectra of CT1, CT2, and CT3 are shown in Fig. 4 indicating that all the samples show distinctive peaks of both CS and TiO_2 in almost similar ranges with a slight variation in their peak intensities. The peaks around 3,741 and 3,848 cm^{-1}, indicate that OH groups of CS have been attached to the TiO_2 network [11]. A broad signal around

Table 1
Average crystallite size and crystal phase of chitosan-TiO_2 (CT1, CT2 and CT3)

Composite sample	CS concentration (g)	Crystalline phase	Crystallite size (nm)
CT1	0.1	Anatase	7.3
CT2	0.2	Anatase	8.4
CT3	0.3	Anatase	10.9

Fig. 2. X-ray diffraction patterns of CT1, CT2, and CT3.
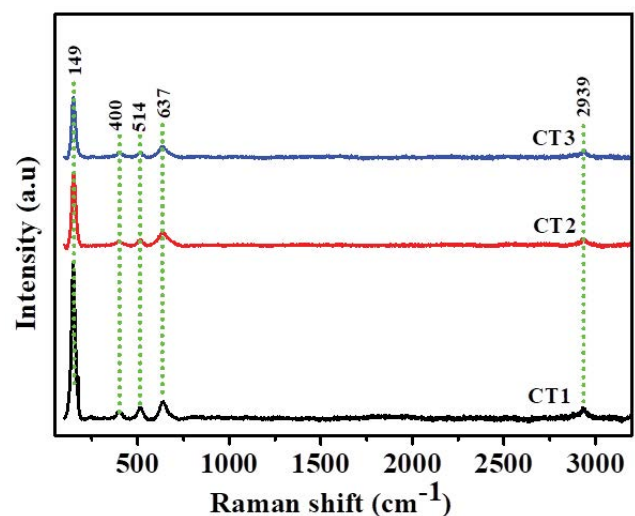
Fig. 3. Raman spectra of CT1, CT2 and CT3.
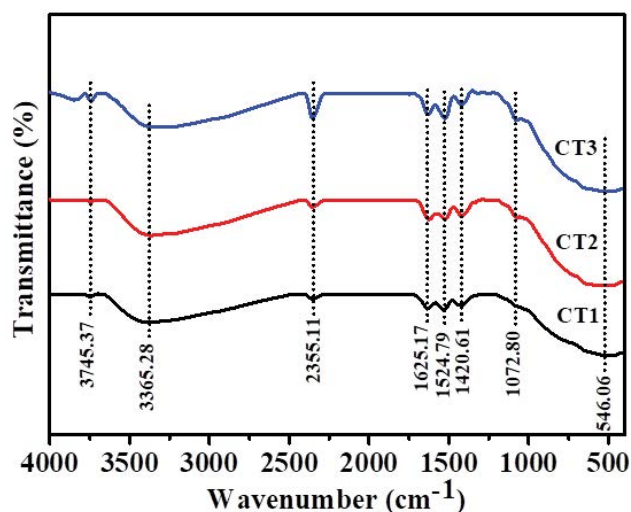
Fig. 4. FTIR spectrum of CT1, CT2 and CT3.

Fig. 5. Photoluminescence spectra of CT1, CT2 and CT3.

~3,300 cm^{-1} is attributed to the stretching vibrations of O–H and N–H groups [18]. A prominent signal at 2,358 cm^{-1} can be correlated to the absorption of CO_2 [19,20]. The N–H bending vibration due to amine groups of CS was observed around 1,625 cm^{-1}. Further the peaks around 1,524 and 1,420 cm^{-1} were corresponds to amide(II) and bending of CH_2 groups of CS [11]. A peak in the range of 1,072 cm^{-1} was assigned to C–O vibrational stretching [21]. Ti–O vibrations and their immobilization in the CS polymeric chains were observed in the spectral range between 400 and 600 cm^{-1}. The three samples show almost consistent results, except their band intensity which is slightly higher at high CS concentrations (CT2 and CT3). In CT1 the lower intensity of groups ranging from 1,072 to 1,625 cm^{-1} corresponds to CS indicating their less availability as a free group and their involvement in bonding with metal oxide (TiO_2) [10,11].

3.5. PL analysis

PL spectra are taken to evaluate the charge carrier separation competency in the composite samples prepared on varying CS loading. All the samples show almost similar peaks with a significant difference in peak intensity Fig. 5. The peak around 330 nm corresponds to ligand to metal charge transfer (O_2 to Ti^{+4}). The second prominent peak observed around 580 nm (CT1) is due to oxygen vacancies and surface defects [22]. However, this peak shifts in CT2 and CT3 to slightly higher wave number, possibly due to the higher concentration of CS. At 663 nm the prominent signals represent red PL which is the migration of trapped electron under CB to VB holes (0.7–1.4 eV) [23].

PL spectra cannot determine the actual position of oxygen [24]; however, high intensity PL peaks are associated with the probability of electron–hole recombination rate [25], while lower PL intensity is associated with better e$^-$ – h$^+$ charge separation [26].

As e$^-$ – h$^+$ recombination rate is generally high on surface defects and in poor crystalline materials [27], therefore, recombination rate increases as crystallinity decreases. This is a possible reason for the lower recombination rate of CT1
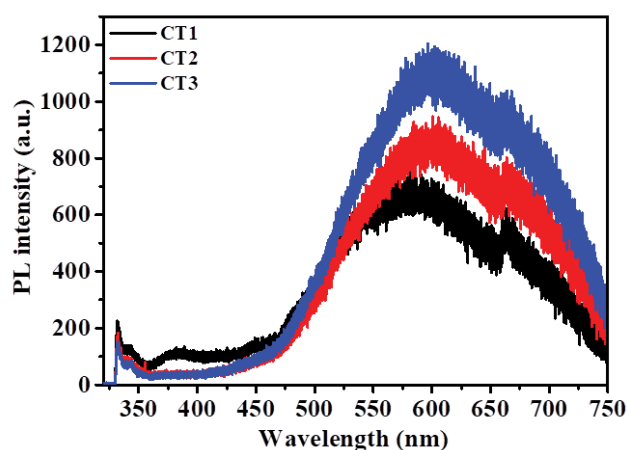
as it shows better crystallinity in comparison to CT2 and CT3 which was also expressed in XRD results. As the intensity of PL spectra is associated with e$^-$ – h$^+$ recombination therefore the sample with lower PL intensity (CT1) is expected to show better performance towards photodegradation. These results are well indexed with the photodegradation of Methyl orange.

3.6. Adsorption photodegradation analysis of Methyl orange via UV-Vis spectroscopy

Fig. 6a and b show the adsorption photodegradation results in the dark and degradation of Methyl orange under UV light. The data illustrates that CT1 shows the complete decolorization (100%) of MO however CT2 and CT3 show 92% and 78%, respectively under UV exposure of 180 min. It indicated, as the concentration of CS increases in the composite, its photocatalytic efficiency decreases gradually. As CS is a semi-crystalline polymer its high concentration increases the roughness of the composite surface and decreases its crystallinity as expressed in SEM and XRD results. Moreover, all three composites show an anatase phase, and increasing CS concentration does not have any effect on the phase but it will reduce crystallinity. The PL data also shows a lower recombination rate of e$^-$ – h$^+$ at lower CS concentrations. Hence, CT1 in comparison to CT2 and CT3 shows the optimum concentration of CS for photocatalytic degradation reactions.

4. Conclusions

Chitosan modified TiO_2 nanocomposite has been synthesized successfully on varying CS concentrations via *in-situ* sol–gel route. Characterization results are well indexed with an anastse crystalline phase of TiO_2 however, crystalline peaks reduce in intensity by increasing CS concentration. The highest adsorption-photodegradation efficiency was shown by CT1, at a low concentration of CS (0.1 g/100 mL) with complete decolorization (100%) of MO within 180 min under UV light. Less availability of free NH_2 and OH groups of CS at lower CS concentration and their involvement in bonding with TiO_2 also enhance
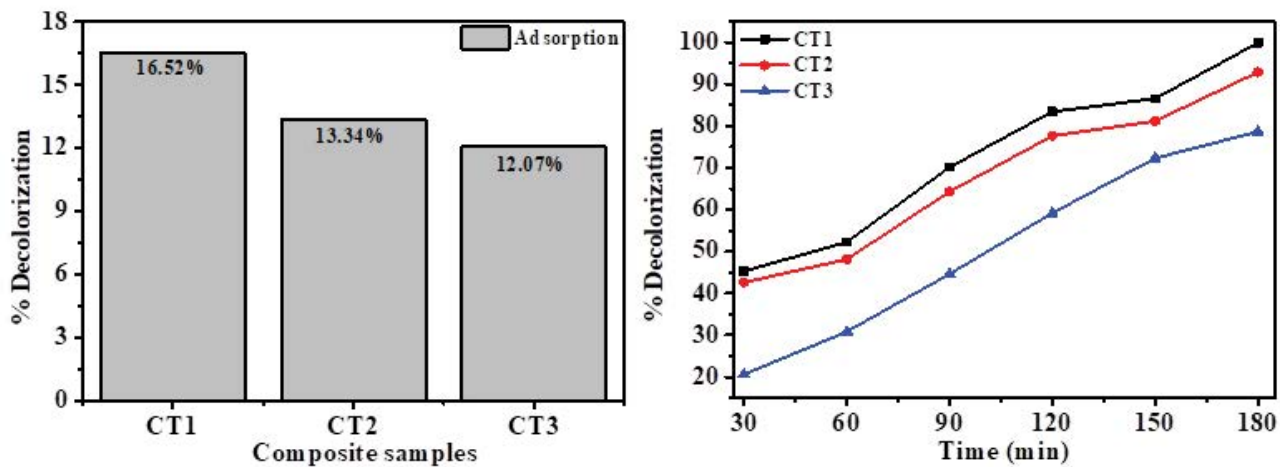
Fig. 6. Photodecolorization of MO by CT1, CT2, and CT3. Percentage adsorption (a) and photodecolorization (b).

its photocatalytic performance. Increasing CS content in composite was reported to reduce the crystallinity and increase the fate of e⁻ – h⁺ recombination. Therefore, CS which is an excellent adsorbent performs well when in low concentration (CT1), giving a better crystalline structure to composite with improved interaction between TiO_2-CS and better charge separation as very well indexed with all the characterization results. The reported optimum concentration of CS helps to design CS based composite of TiO_2 for the photodegradation of a variety of pollutants.

References

[1] K. Thangavelu, R. Annamalai, D. Arulnandhi, Preparation and characterization of nanosized TiO_2 powder by sol–gel precipitation route, Int. J. Emerg. Technol. Adv. Eng., 3 (2013) 636–639.

[2] D. Siamak, F. Moslem, N. Mohammad, Solid state dispersion and hydrothermal synthesis, characterization and evaluations of TiO_2/ZnO nanostructures for degradation of Rhodamine B, Desal. Water Treat., 231 (2021) 425–435.

[3] M.H. Farzana, S. Meenakshi, Synergistic effect of chitosan and titanium dioxide on the removal of toxic dyes by the photodegradation technique, Ind. Eng. Chem. Res., 53 (2014) 55–63.

[4] S.H. Othman, T.I.M. Ghazi, S.A. Rashid, N. Abdullah, Dispersion and stabilization of photocatalytic TiO_2 nanoparticles in aqueous suspension for coatings applications, J. Nanomater., 2012 (2012) 718214, doi: 10.1155/2012/718214.

[5] S. Bagheri, N. Muhd Julkapli, S.B. Abd Hamid, Titanium dioxide as a catalyst support in heterogeneous catalysis, Sci. World J., 2014 (2014) 727496, doi: 10.1155/2014/727496.

[6] S.M. Gupta, M. Tripathi, A review of TiO_2 nanoparticles, Chin. Sci. Bull., 56 (2011) 1639–1657.

[7] Y. Haldorai, Chitosan/titanium oxide composite: a photocatalyst and bacteriocide, SPE, (2013).

[8] A.P. Hossein, F. Moslem, K.-N. Mohammadreza, Synthesis and characterization of ternary chitosan–TiO_2–ZnO over graphene for photocatalytic degradation of tetracycline from pharmaceutical wastewater, Sci. Rep., 11 (2021) 24177, doi: 10.1038/s41598-021-03492-5.

[9] A. Nithya, K. Jothivenkatachalam, Visible light assisted TiO_2-chitosan composite for removal of reactive dye, J. Environ. Nanotechnol., 3 (2014) 20–26.

[10] I. Fajriati, M. Mudasir, E.T. Wahyuni, Photocatalytic decolorization study of Methyl orange by TiO_2-chitosan nanocomposites, Indonesian J. Chem., 14 (2014) 209–218.

[10] S. Afzal, E.M. Samsudin, N.M. Julkapli, S.B.A. Hamid, Controlled acid catalyzed sol–gel for the synthesis of highly active TiO_2-chitosan nanocomposite and its corresponding photocatalytic activity, Environ. Sci. Pollut. Res., 23 (2016) 23158–23168.

[11] S. Afzal, E.M. Samsudin, L.K. Mun, N.M. Julkapli, S.B.A. Hamid, Room temperature synthesis of TiO_2 supported chitosan photocatalyst: study on physicochemical and adsorption photo-decolorization properties, Mater. Res. Bull., 86 (2017) 24–29.

[12] M. Hema, A. Yelil Arasi, P. Tamilselvi, R. Anbarasan, Titania nanoparticles synthesized by sol–gel technique, Chem. Sci. Trans., 2 (2013) 239–245.

[13] C.S. Lim, J.H. Ryu, D.-H. Kim, S.-Y. Cho, W.C. Oh, Reaction morphology and the effect of pH on the preparation of TiO_2 nanoparticles by a sol–gel method, J. Ceram. Process. Res., 11 (2010) 736–741.

[14] D. Li, H. Song, X. Meng, T. Shen, J. Sun, W. Han, X. Wang, Effects of particle size on the structure and photocatalytic performance by alkali-treated TiO_2, Nanomaterials (Basel, Switzerland), 10 (2020) 546, doi: 10.3390/nano10030546.

[15] E.M. Simonsen, E.G. Søgaard, Sol–gel reactions of titanium alkoxides and water: influence of pH and alkoxy group on cluster formation and properties of the resulting products, J. Sol-Gel Sci. Technol., 53 (2010) 485–497.

[16] H.C. Choi, Y.M. Jung, S.B. Kim, Size effects in the Raman spectra of TiO_2 nanoparticles, Vib. Spectrosc., 37 (2004) 33–38.

[17] D.A. Gómez, J. Coello, S. Maspoch, The influence of particle size on the intensity and reproducibility of Raman spectra of compacted samples, Vib. Spectrosc., 100 (2019) 48–56.

[18] M. Safari, M. Ghiaci, M. Jafari-Asl, A.A. Ensafi, Nanohybrid organic–inorganic chitosan/dopamine/TiO_2 composites with controlled drug-delivery properties, Appl. Surf. Sci., 342 (2015) 26–33.

[19] E.M. Samsudin, S.B. Abd Hamid, J.C. Juan, W.J. Basirun, A.E. Kandjani, S. Bhargava, Controlled nitrogen insertion in titanium dioxide for optimal photocatalytic degradation of atrazine, RSC Adv., 5 (2015) 44041–44052.

[20] R.V. da Silva Amorim, W. de Souza, K. Fukushima, G.M. de Campos-Takaki, Faster chitosan production by mucoralean strains in submerged culture, Braz. J. Microbiol., 32 (2001) 20–23.

[21] R. Jiang, H.Y. Zhu, H.H. Chen, J. Yao, Y.-Q. Fu, Z.Y. Zhang, Y.M. Xu, Effect of calcinations temperature on physical parameters and photocatalytic activity of mesoporous titania spheres using chitosan/poly(vinyl alcohol) hydrogel beads as a template, Appl. Surf. Sci., 319 (2014) 189–196.

[22] Z. Jin, W. Duan, B. Liu, X. Chen, F. Yang, J. Guo, Indium doped and carbon modified P25 nanocomposites with high visible-light sensitivity for the photocatalytic degradation of organic dyes, Appl. Catal., A, 517 (2016) 129–140.

[23] E.M. Samsudin, S.B.A. Hamid, J.C. Juan, W.J. Basirun, Influence of triblock copolymer (pluronic F127) on enhancing the physico-chemical properties and photocatalytic response of mesoporous TiO$_2$, Appl. Surf. Sci., 355 (2015) 959–968.

[24] M. Kong, Y. Li, X. Chen, T. Tian, P. Fang, F. Zheng, X. Zhao, Tuning the relative concentration ratio of bulk defects to surface defects in TiO$_2$ nanocrystals leads to high photocatalytic efficiency, J. Am. Chem. Soc., 133 (2011) 16414–16417.

[25] R. Zha, R. Nadimicherla, X. Guo, Ultraviolet photocatalytic degradation of Methyl orange by nanostructured TiO$_2$/ZnO heterojunctions, J. Mater. Chem. A, 3 (2015) 6565–6574.

[26] A.H. Jawad, M.A. Nawi, Oxidation of crosslinked chitosan-epichlorohydrine film and its application with TiO$_2$ for phenol removal, Carbohydr. Polym., 90 (2012) 87–94.

[27] S.M. Gupta, M. Tripathi, A review of TiO$_2$ nanoparticles, Chin. Sci. Bull., 56 (2011) 1639–1657.